Article

Molecular Cell

# Structural Basis for the Activation and Inhibition of the UCH37 Deubiquitylase

## Graphical Abstract

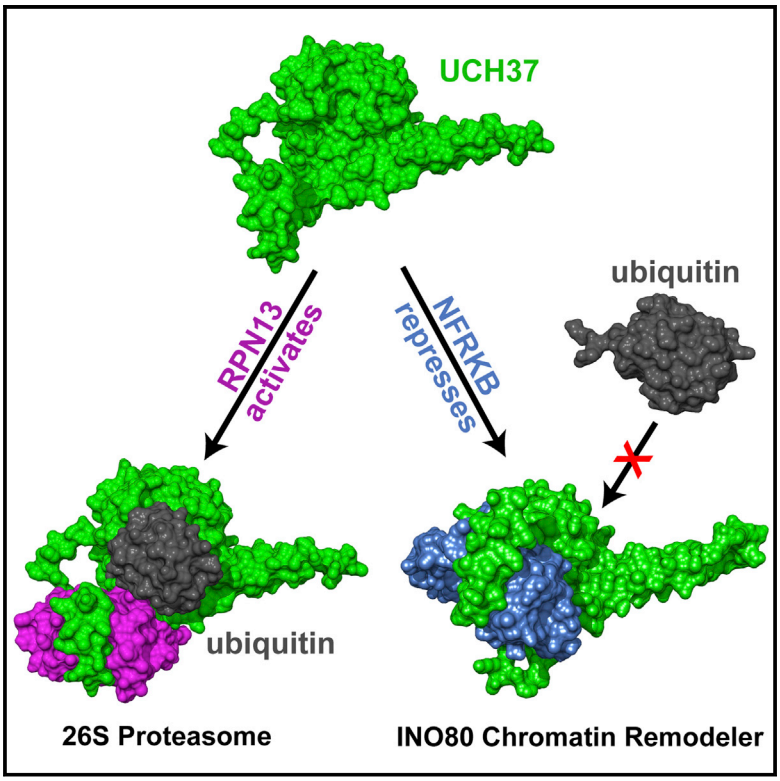


## Authors

Ryan T. VanderLinden,
Casey W. Hemmis, ..., Tingting Yao,
Christopher P. Hill

## Correspondence

tingting.yao@colostate.edu (T.Y.),
chris@biochem.utah.edu (C.P.H.)

## In Brief

VanderLinden et al. determined structures and performed biochemical studies of the essential deubiquitylase UCH37 with its 26S proteasome and INO80 chromatin remodeler binding partners. The mechanistic basis for how UCH37 is activated in the proteasome complex but repressed in the INO80 complex is explained.

## Highlights

- The DUB UCH37 is a subunit of the 26S proteasome and the INO80 chromatin remodeler
- Proteasome/RPN13 and INO80/NFRKB bind similarly to the UCH37 C-terminal helices
- RPN13 activates UCH37 through contacts that enhance ubiquitin binding
- NFRKB inhibits UCH37 by occluding ubiquitin binding and disrupting the active site

## Accession Numbers

4WLP
4WLQ
4WLR

VanderLinden et al., 2015, Molecular Cell *57*, 901–911
March 5, 2015 ©2015 Elsevier Inc.
http://dx.doi.org/10.1016/j.molcel.2015.01.016

CrossMark

CellPress

Molecular Cell
Article

# Structural Basis for the Activation and Inhibition of the UCH37 Deubiquitylase

Ryan T. VanderLinden,[1,4] Casey W. Hemmis,[1,4] Benjamin Schmitt,[2] Ada Ndoja,[2] Frank G. Whitby,[1] Howard Robinson,[3] Robert E. Cohen,[2] Tingting Yao,[2,*] and Christopher P. Hill[1,*]
[1]Department of Biochemistry, University of Utah School of Medicine, Salt Lake City, UT 84112-5650, USA
[2]Department of Biochemistry and Molecular Biology, Colorado State University, Fort Collins, CO 80523, USA
[3]Biology Department, Brookhaven National Laboratory, Upton, NY 11973, USA
[4]Co-first author
*Correspondence: tingting.yao@colostate.edu (T.Y.), chris@biochem.utah.edu (C.P.H.)
http://dx.doi.org/10.1016/j.molcel.2015.01.016

## SUMMARY

**The UCH37 deubiquitylase functions in two large and very different complexes, the 26S proteasome and the INO80 chromatin remodeler. We have performed biochemical characterization and determined crystal structures of UCH37 in complexes with RPN13 and NFRKB, which mediate its recruitment to the proteasome and INO80, respectively. RPN13 and NFRKB make similar contacts to the UCH37 C-terminal domain but quite different contacts to the catalytic UCH domain. RPN13 can activate UCH37 by disrupting dimerization, although physiologically relevant activation likely results from stabilization of a surface competent for ubiquitin binding and modulation of the active-site crossover loop. In contrast, NFRKB inhibits UCH37 by blocking the ubiquitin-binding site and by disrupting the enzyme active site. These findings reveal remarkable commonality in mechanisms of recruitment, yet very different mechanisms of regulating enzyme activity, and provide a foundation for understanding the roles of UCH37 in the unrelated proteasome and INO80 complexes.**

## INTRODUCTION

Covalent attachment of ubiquitin to target proteins has a profound impact on numerous cellular pathways, including protein quality control, cell-cycle progression, signal transduction, endocytosis, transcription, and DNA repair (Pickart, 2001). Integral to regulation of these pathways is the reverse process of removing ubiquitin, which is performed by the nearly 100 deubiquitylating enzymes (DUBs) that have been identified in the human genome (Nijman et al., 2005). DUBs have been classified into five protein families (Clague et al., 2012). The topic of this study, UCH37, also known as UCHL5, is one of the four members of the human UCH (ubiquitin C-terminal hydrolase) family of DUBs.

Remarkably, UCH37 is a subunit of two strikingly different complexes: INO80 (Yao et al., 2008), which performs ATP-dependent sliding of nucleosomes for transcriptional regulation and DNA repair (Cai et al., 2007; Wu et al., 2007), and the 26S proteasome (Hölzl et al., 2000; Lam et al., 1997; Li et al., 2000), which performs ATP-dependent proteolysis of polyubiquitylated proteins in the cytosol and nucleus (Varshavsky, 2005). Recruitment of UCH37 to these complexes depends on its autoinhibitory C-terminal domain ($UCH37^{CTD}$) (Yao et al., 2006, 2008), which follows the N-terminal catalytic UCH domain ($UCH37^{UCH}$) that contains the active-site residues and binds ubiquitin (Burgie et al., 2012; Maiti et al., 2011; Morrow et al., 2013; Nishio et al., 2009) in the same manner as that of other UCH enzymes (Boudreaux et al., 2010; Johnston et al., 1997, 1999). It is not known which of these complexes, which appear to have no other subunits in common, mediates the essential UCH37 function that results in (1) embryonic lethality due to severe defects in brain development upon genomic deletion of *Uch37* in mice (Al-Shami et al., 2010) and (2) its implication in multiple cancers (Chen et al., 2012; Fang et al., 2012; Wang et al., 2014). Regardless, the potential of UCH37 as a therapeutic target has been noted (Chen et al., 2013; Cutts et al., 2011; D'Arcy et al., 2011).

It was previously reported that isolated full-length UCH37 displays only weak activity against the model substrate ubiquitin-AMC, whereas C-terminally truncated $UCH37^{UCH}$ variants display robust activity (Yao et al., 2006). Recruitment to the proteasome is mediated by RPN13 (also known as ADRM1), whose C-terminal domain ($RPN13^{CTD}$) binds the $UCH37^{CTD}$ and greatly stimulates activity against model substrates (Hamazaki et al., 2006; Qiu et al., 2006; Yao et al., 2006), whereas the RPN13 N-terminal domain binds the large proteasome scaffolding subunit RPN2 (Chen et al., 2010b). Recruitment to INO80 is mediated by the N-terminal domain of NFRKB ($NFRKB^{NTD}$), which also binds the $UCH37^{CTD}$ and, in sharp contrast to RPN13, further inhibits UCH37 activity (Yao et al., 2008). NFRKB presumably makes additional interactions with INO80 components, although those contacts have not yet been characterized. Curiously, INO80-associated UCH37 can be activated by transient incubation with either RPN13 or 26S proteasome lacking UCH37, without UCH37 dissociating from the INO80 complex (Yao et al., 2008).

In an effort to understand UCH37 recruitment to the proteasome and INO80, and the very different consequences that these complexes have on deubiquitylation activity, we have determined crystal structures of full-length UCH37 in three

complexes: with RPN13$^{CTD}$, with RPN13$^{CTD}$ and ubiquitin, and with NFRKB$^{NTD}$. These structures and associated biochemical analyses reveal that RPN13 and NFRKB make similar interactions with the UCH37$^{CTD}$ but have very different interactions with the catalytic UCH domain that are activating in the case of RPN13 and highly inhibitory in the case of NFRKB. These findings demonstrate how protein-protein interactions activate or inhibit UCH37 and provide a foundation for deciphering UCH37's distinct roles and regulation in the 26S proteasome and in INO80.

## RESULTS

### Structure Determinations

Complexes with human UCH37 did not yield crystals with good diffraction properties, whereas crystals of murine UCH37 (isoform 2) and human RPN13$^{285-407}$ diffracted well. The murine and human UCH37 proteins share 96% sequence identity, and, as subsequently revealed, all of the residues at the interfaces with RPN13 and ubiquitin are identical. The structure was determined by a combination of molecular replacement using the previously reported structure of UCH37 (Protein Data Bank [PDB] ID: 3IHR) (Burgie et al., 2012) and single-wavelength anomalous diffraction (SAD) using a complex containing selenomethionine (SeMet)-substituted RPN13. This structure was refined to $R_{work}/R_{free}$ values of 27.6%/32.5% against data to a resolution of 3.2 Å (data not shown). The resulting model revealed that RPN13 residues 385–407 were disordered in the crystals, which prompted efforts with a truncated construct spanning residues 285–386 (hereinafter, RPN13$^{CTD}$). These crystals diffracted to 2.85 Å resolution, and the structure was refined to $R_{work}/R_{free}$ values of 19.2%/27.8%.

To understand how UCH37-RPN13$^{CTD}$ recognizes its substrate, we crystallized a ternary complex with human ubiquitin, collected data to 2.0 Å resolution, and refined this structure to $R_{work}/R_{free}$ values of 18.1%/22.7%. All three of these structures belong to space group $P2_12_12_1$, have similar cell dimensions, and contain one copy of the complex in the asymmetric unit. Only minimal changes were evident upon binding of ubiquitin. Superposition of UCH37-RPN13$^{CTD}$ in the presence and absence of ubiquitin yields a root-mean-square deviation of 1.29 Å over all 385 pairs of Cα atoms, with the maximal change of 6.8 Å found in an inherently flexible loop of UCH37 at the ubiquitin interface. Because of this high degree of similarity, remarks and figures will refer to the higher resolution ternary complex.

Several different NFRKB constructs were subjected to crystallization trials. Isomorphous crystals were obtained with full-length human UCH37 isoforms 1 and 2, with the best data obtained with isoform 2 in complex with NFRKB$^{39-156}$. The structure was determined by molecular replacement using UCH37$^{1-228}$ as the search model. The SeMet-NFRKB$^{NTD}$ mutant proteins L62M and L92M were used to verify model building by inspection of anomalous difference maps. This structure was refined to $R_{work}/R_{free}$ values of 19.3%/26.8% against data to 3.1 Å resolution. Crystallographic statistics for all structures are given in Table 1.

Although our crystal structures used mouse or human UCH37 isoform 2, most of the biochemical studies were performed with human UCH37 isoform 1, which differs from the isoform 2 protein only in the inclusion of an additional glutamate (E246) in the flexible loop between helices α8 and α9. This introduces an ambiguity in numbering for UCH37 residues 246–328 (C terminus), which is addressed explicitly when relevant. Analytical ultracentrifugation (AUC) and kinetic studies performed with isoform 2 UCH37 gave results indistinguishable from those of isoform 1, but the isoform 2 protein was more prone to aggregation and, therefore, was more limited in the range of conditions that could be assayed.

### Overall Structures

UCH37 (Figure 1A) comprises a catalytic UCH domain (UCH37$^{UCH}$) followed by the four-helix (α8–α11) C-terminal domain (UCH37$^{CTD}$). Helices α8 and α9 pack against each other in a hairpin structure. Helices α10 and α11 do not make intramolecular contacts but are stabilized by packing against an adjacent UCH37 molecule in the unliganded structure (Burgie et al., 2012) or by packing against RPN13 or NFRKB in the structures reported here. The catalytic UCH domain structures of both the RPN13$^{CTD}$ and NFRKB$^{NTD}$ complexes are generally very similar to that of unliganded UCH37, with differences concentrated at interfaces with ubiquitin, RPN13, and NFRKB. The 21-residue active-site crossover loop (ASCL), which is a distinctive feature of UCH enzymes and is substantially disordered in all of the UCH37 structures, arches over the active site and spans the ubiquitin C terminus.

The UCH37 active-site structure is highly conserved in the RPN13$^{CTD}$ complex, and contacts to ubiquitin superimpose closely with those of the isolated *Trichinella spiralis* UCH37$^{UCH}$ domain in complex with ubiquitin vinyl methyl ester (Morrow et al., 2013) and other UCH enzymes with ubiquitin aldehyde or ubiquitin vinyl methyl ester (Artavanis-Tsakonas et al., 2010; Boudreaux et al., 2010; Johnston et al., 1999; Misaghi et al., 2005) (Figure 1B). As expected, the catalytic cysteine side chain is turned away from the ubiquitin carboxylate in order to accommodate formation of the product complex. There are hints in the density that could be interpreted as a minor fraction of the covalently attached acyl intermediate, although attempts to model and refine this minor conformation gave occupancies of less than 10%; therefore, we describe the structure as a single conformation of the enzyme-product complex.

Overviews of the RPN13$^{CTD}$ and NFRKB$^{NTD}$ complexes are shown in Figures 2A and 2B. RPN13$^{CTD}$ undergoes substantial refolding from its unbound conformation (Chen et al., 2010b) to form extensive, mostly hydrophobic, contacts with the last two turns of UCH37 α9, α10, and one side of α11 (Figure 2C). Like RPN13$^{CTD}$, NFRKB$^{NTD}$ comprises a series of helices, with the first 5 helices of RPN13$^{CTD}$ and NFRKB$^{NTD}$ making equivalent interactions with the UCH37$^{CTD}$ (Figure 2D). Guided by the Dali server (Holm and Rosenström, 2010), inspection of the structures indicates that almost all of the residues from the beginning of α1 to shortly after α5 are structurally equivalent between RPN13$^{CTD}$ and NFRKB$^{NTD}$, with the most notable exception being the F100 loop of NFRKB (Figures 2D and 2E), which is a six-residue insertion relative to RPN13. Despite this structural similarity, only 8 (13.5%) of the 59 structurally equivalent residues have the same amino acid identity in RPN13 and NFRKB. Following α5, the paths of RPN13$^{CTD}$ and NFRKB$^{NTD}$ diverge

**Table 1. Data Collection and Refinement Statistics**

| | mUCH37-RPN13$^{CTD}$ | mUCH37-RPN13$^{CTD}$-Ubiquitin | hUCH37-NFRKB$^{NTD}$ |
|---|---|---|---|
| Data Collection | | | |
| Space group | $P2_12_12_1$ | $P2_12_12_1$ | $P4_122$ |
| Cell dimensions | | | |
| *a*, *b*, *c* (Å) | 59.95, 96.95, 99.34 | 60.12, 99.61, 99.91 | 95.49, 95.49, 132.00 |
| α, β, γ(°) | 90.0, 90.0, 90.0 | 90.0, 90.0, 90.0 | 90.0, 90.0, 90.0 |
| Resolution (Å) | 40.00–2.85 (3.00–2.85) | 40.00–2.00 (2.05–2.00) | 40.00–3.10 (3.32–3.10) |
| $R_{pim}$[a] | 0.042 (0.375) | 0.024 (0.556) | 0.038 (0.433) |
| I/σI | 12.2 (2.4) | 17.7 (1.5) | 17.6 (2.0) |
| Completeness (%) | 100.0 (100.0) | 99.7 (96.2) | 99.9 (100.0) |
| Redundancy | 7.9 (7.6) | 14.5 (13.7) | 12.9 (12.9) |
| CC1/2 | 0.996 (0.861) | 0.998 (0.589) | 1.000 (0.638) |
| Refinement | | | |
| Resolution (Å) | 40.00–2.85 (3.00–2.85) | 40.00–2.00 (2.05–2.00) | 40.00–3.10 (3.27–3.10) |
| Number of reflections | 13,952 (1,372) | 41,279 (2,639) | 11,605 (1,466) |
| $R_{work}/R_{free}$ | 0.192 (0.292)/0.278 (0.411) | 0.181 (0.332)/0.227 (0.425) | 0.193 (0.254)/0.268 (0.299) |
| Number of atoms | | | |
| Protein | 3,082 | 3,719 | 3,352 |
| Water | 0 | 201 | 0 |
| B-factors | | | |
| Protein | 112.4 | 58.7 | 95.8 |
| Water | 0 | 50.3 | 0 |
| Rmsds | | | |
| Bond lengths (Å) | 0.009 | 0.008 | 0.009 |
| Bond angles (°) | 1.21 | 1.07 | 1.11 |

One crystal was used for each of the data collections. Values in parentheses are for the highest resolution shell. Rmsds, root-mean-square deviations. [a]$R_{pim}$, precision-indicating merging factor, is a statistic similar to $R_{meas}$ that indicates the quality of data (Weiss, 2001) and is calculated as: $Rpim = \sum_{hkl}\left[\frac{1}{(N-1)}\right]^{\frac{1}{2}}\sum_i |I_i(hkl) - \overline{I(hkl)}|/\sum_{hkl}\sum_i I_i(hkl)$.

dramatically, with RPN13$^{CTD}$ forming a three-helix bundle that packs against the side of UCH37 α10 opposite that of RPN13 α2, α3, and α4, whereas NFRKB$^{NTD}$ forms a single, long helix that lies against the UCH37$^{UCH}$ domain.

Despite the similarities in the interactions with the UCH37$^{CTD}$, the overall structures of the RPN13$^{CTD}$ and NFRKB$^{NTD}$ complexes display gross differences. These different conformations are driven by distinct interactions that RPN13$^{CTD}$ and NFRKB$^{NTD}$ make with the UCH37$^{UCH}$ domain, which induce different orientations of UCH37$^{CTD}$ helices α8–α11 with respect to the UCH domain (Figure 2F). Overlap of the UCH37$^{UCH}$ domains reveals that this conformational change comprises an ~30° tilt for α8 and the N-terminal region of α9 and an ~45° kink in α9 at R279 (Figure 2G). As discussed later, the differences in UCH domain contacts and the attendant orientations of the CTD helices explain the activation of UCH37 by RPN13 and its inhibition by NFRKB.

## RPN13 Disrupts a UCH37 Dimer at High Concentration

The RPN13 complex structure is consistent with the leading model that activation results from disruption of an inhibitory dimer (Jiao et al., 2014). UCH37 oligomerizes in a concentration-dependent manner and crystallizes in the absence of a binding partner as a dimer of dimers (Burgie et al., 2012). Although this point has been controversial, recent studies with SAXS and FRET have further reported that binding of RPN13 disrupts oligomerization to activate UCH37 (Jiao et al., 2014). This is attractive because binding of RPN13 and ubiquitin, as seen in our complex crystal structures, is incompatible with formation of the largest dimer interface seen in crystals of unliganded UCH37 (Figure 3A). We have advanced these studies by using equilibrium AUC to demonstrate that full-length UCH37 dimerizes with a dissociation constant, $K_D$, of 2.7 μM (Figure 3B). Consistent with the packing of α9 and α10 at the dimer interface, we found that the isolated UCH domain (UCH37$^{UCH(1–228)}$) is monomeric (Figure 3C). Because of the details of packing and the large size of the interface (4,100 Å$^2$), it was challenging to design point mutants that would selectively disrupt the association without otherwise compromising the structure. Nevertheless, we found that the double mutant M269E, N291D (corresponds to M268 and N290 of the isoform 2 UCH37 in the crystal structures) weakens dimerization ~20-fold to a $K_D$ of 49 μM (Figure 3D), thereby further validating the crystallographic dimer interface. As expected from the model, we demonstrated that binding of RPN13 results in formation of a stable 1:1 heterodimer (Figure 3E).

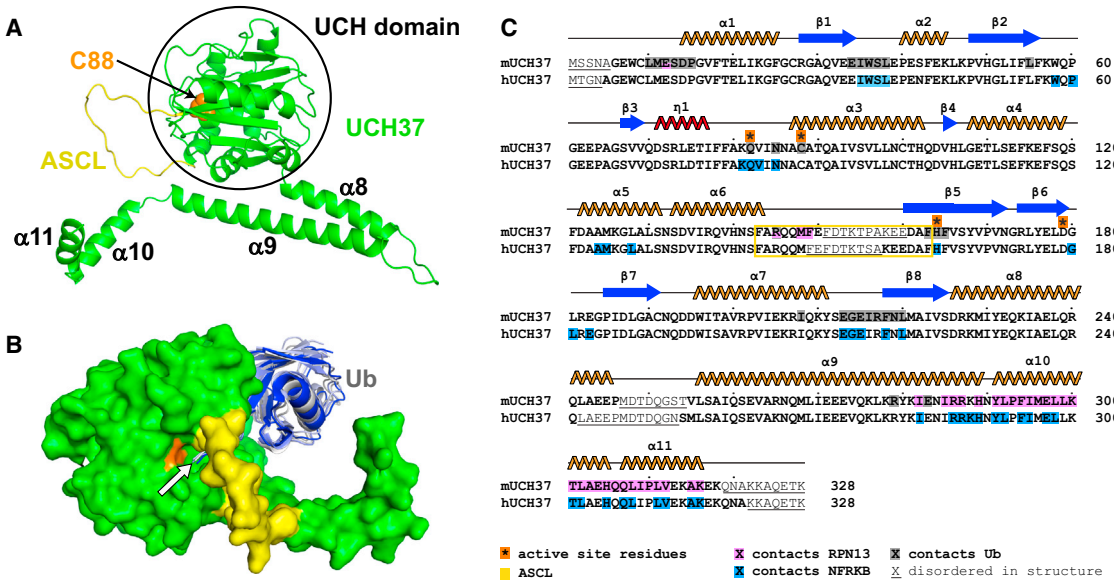


**Figure 1. Structure of UCH37 and Ubiquitin Complex**

(A) UCH37, ribbon representation, as seen in the RPN13 complexes. The catalytic C88 is shown as orange spheres; ASCL, yellow. Helices α8–α11 that constitute the CTD are labeled.

(B) Surface representation of UCH37 with ubiquitin (shades of blue-gray) from the RPN13 complex and structures of ubiquitin in complex with other UCH family members (Boudreaux et al., 2010; Johnston et al., 1999; Misaghi et al., 2005; Morrow et al., 2013) following superposition on the UCH domains. The ubiquitin C terminus is indicated with an arrow.

(C) Sequence and secondary structures of murine UCH37 isoform 2 (RPN13 and ubiquitin complex) and human UCH37 isoform 2 (NFRKB complex).

Although an autoinhibitory role for UCH37 dimerization is established under some biochemical conditions, the observed micromolar dissociation constant suggests that dimerization should not be relevant at the nanomolar concentration of UCH37 in standard ubiquitin-AMC hydrolysis assays, where the autoinhibitory effect of the UCH37 C-terminal domain was first observed (Yao et al., 2006). Therefore, we performed similar ubiquitin-AMC hydrolysis assays and found negligible difference in activity between full-length UCH37 and UCH37$^{UCH(1–228)}$ (Table 2), thereby verifying that inhibitory dimerization or other CTD-mediated autoinhibition is not relevant under these conditions. Consistent with another report (Maiti et al., 2011), a likely explanation is that the original studies (Yao et al., 2006) used glutathione S-transferase (GST)-UCH37 constructs and that the observed inhibition was driven by GST dimerization (Fabrini et al., 2009). These observations indicate that dimerization through the UCH37$^{CTD}$ is inhibitory at micromolar concentrations but argues against the possibility that this mechanism is relevant under physiological conditions. Moreover, we have been unable to detect UCH37 dimers in cultured mammalian cells (data not shown).

## Activation of UCH37 by RPN13$^{CTD}$

The UCH37-RPN13$^{CTD}$ complex displays 8-fold greater catalytic efficiency than isolated UCH37 or UCH37$^{UCH(1–228)}$ (Table 2). Inspection of the structure (Figure 4) indicates that this does not result from changes at the active site, because the nearest RPN13 atom is ~18 Å from the UCH37 catalytic center, and the oxyanion-intermediate stabilizing residue Q82, nucleophilic C88, activating H164, and associated D179 are all essentially unchanged upon RPN13 binding (Burgie et al., 2012). Rather, activation is explained by contacts of RPN13 with the UCH37$^{UCH}$ domain, which are limited to residues E12, R145, M148, and F149 (Figure 4B). The UCH37 M148A and F149A double mutation results in kinetic parameters that are indistinguishable from those of unbound UCH37 (Table 2), indicating that this contact is indeed required for activation, probably because it functions to promote ubiquitin binding by stabilizing UCH37 α9 in an orientation that favors ubiquitin binding and positions RPN13 Q337 and Q338 for direct contacts with ubiquitin (Figure 4C). Activation resulting from improved ubiquitin binding is also consistent with the dominant effect of the Michaelis-Menten constant, $K_M$, while the modest 2.5-fold effect of the RPN13 Q337A and Q338A double mutation supports the interpretation that the improved binding results from multiple interactions. RPN13 also likely facilitates productive binding by holding residues at the N terminus of the ASCL in an orientation projecting away from the UCH domain, thereby promote an open conformation of the ASCL (Figure 4A). Although this is unlikely to have a major impact on hydrolysis of very small ubiquitin adducts, such as ubiquitin-AMC, it may have important consequences for processing larger, physiological substrates.

## Inhibition of UCH37 by NFRKB$^{NTD}$

NFRKB$^{NTD}$ inhibits UCH37 because of two distinct contacts that it makes with the UCH domain. In one of these contacts, four residues of the highly conserved F100 loop (residues $^{97}$NFRF$^{100}$) bind in the UCH37 pocket that is lined by UCH37 residues L38, I208, F218, and L220. This pocket binds the ubiquitin L8 turn in the UCH37-RPN13-ubiquitin complex,

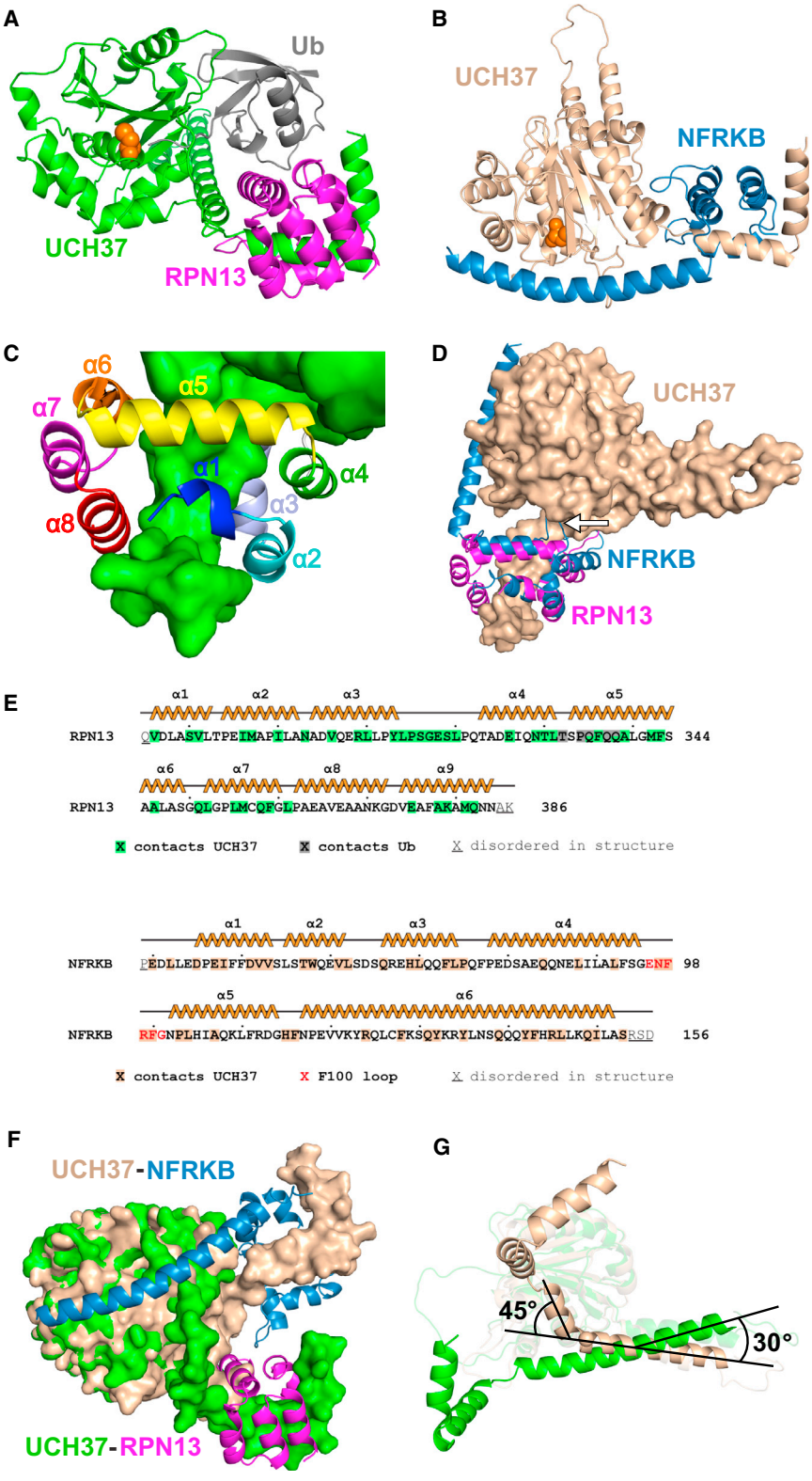


**Figure 2. Structures of RPN13 and NFRKB Complexes**

(A) Overview of the RPN13-UCH37-ubiquitin complex.

(B) Overview of the NFRKB-UCH37 complex. (A) and (B) show the same relative orientation for UCH37 residues from the last two turns of α9 to the end of α11.

(C) RPN13 with helices labeled.

(D) Superposition of RPN13 and NFRKB following alignment of the C-terminal residues of UCH37 α9, α10, and α11. The F100 loop of NFRKB is indicated by an arrow.

(E) RPN13 and NFRKB sequences and secondary structures. All residues in the crystallized constructs are indicated.

(F) Surface representation of RPN13$^{CTD}$ and NFRKB$^{NTD}$ complexes overlapped on the catalytic UCH domain. RPN13$^{CTD}$ and NFRKB$^{NTD}$ shown as ribbons. For clarity, ubiquitin is not shown.

(G) Ribbon representation, viewed orthogonally to (A). The 30° tilt of α8 and α9 and the 45° kink in α9 are indicated. RPN13 and NFRKB are not shown. R279 CA is indicated with a sphere.

indicating that the NFRKB F100 loop blocks ubiquitin binding directly (Figure 5A). This contact also places NFRKB and the UCH37$^{CTD}$ against the UCH37$^{UCH}$ domain in a position that completely disrupts and occludes the ubiquitin-binding site (Figure 5B).

NFRKB also makes an inhibitory contact through the packing of its C-terminal helix against the UCH domain (Figures 2B and 5C). This relatively long helix resembles a clasp whose binding energy helps lock the residues of the NFRKB F100 loop in their inhibitory position against the UCH37$^{UCH}$ domain. In contrast to the RPN13 complex, which shows an active-site geometry that is essentially unchanged from the unliganded structure, the extensive interface formed by the NFRKB$^{NTD}$ C-terminal helix distorts the active site. The CA atom of the catalytic residue H164 is displaced by 2.3 Å, and its side chain rotates ~90° about the CA-CB bond to give a 4.5-Å side chain displacement that is stabilized by hydrogen bonding with NFRKB Y135. This specific disruption of a key catalytic residue is coupled to restructuring of multiple UCH37 residues that contact NFRKB. Of particular note, the consequent repositioning of A162 and F163 occludes the active-site cleft that binds the C-terminal residues of ubiquitin in the RPN13 complex (Figure 5D).

Consistent with the structure, the UCH37-NFRKB$^{NTD}$ complex hydrolyzes ubiquitin-AMC with 270-fold reduced catalytic efficiency compared to the UCH37-RPN13$^{CTD}$ complex, resulting from an ~5-fold higher $K_M$ and ~50-fold lower catalytic rate constant,

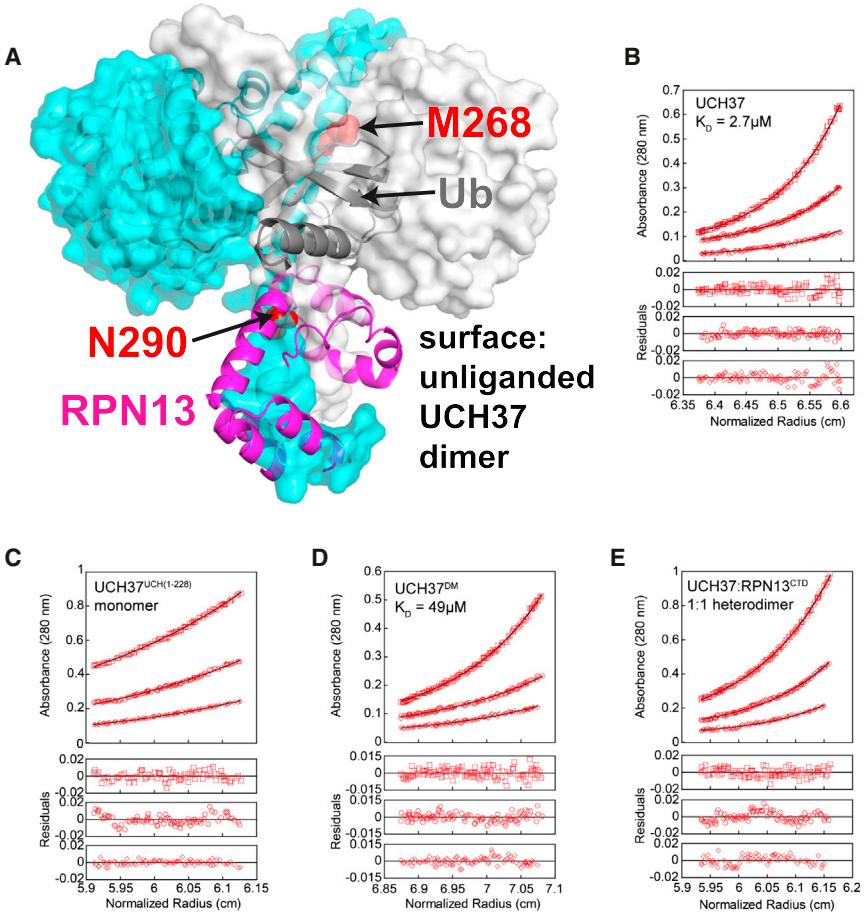


**Figure 3. Regulation of UCH37 by Dimerization**

(A) Structure of the largest dimer interface from crystals of unliganded UCH37 (PDB ID: 3IHR) (Burgie et al., 2012). Each subunit is shown as a transparent surface. Ubiquitin and RPN13$^{CTD}$ (ribbons) from the complex structure are superimposed on the left subunit. Residues mutated to destabilize the interface (M269/N291, isoform 1) are shown as red spheres.

(B–E) Equilibrium AUC analysis. Data are shown for the highest rotor speed (13,000 rpm) with the global fit for all data (black line) indicated. (B) UCH37 (monomer-dimer equilibrium). (C) UCH37$^{UCH(1–228)}$. Floating molecular weight (MW) fit yielded 24,595 Da, compared to the calculated mass of 25,673 Da, for an $MW_{obs}/MW_{calc}$ of 0.96, consistent with a monomer. $MW_{obs}$ indicates the observed/experimental MW derived from our studies. $MW_{calc}$ indicates the expected MW based on amino acid composition of the protein(s) used. (D) UCH37(M269E,N291D)/UCH37$^{DM}$ (monomer-dimer equilibrium). (E) UCH37-RPN13$^{285–407}$. Floating molecular weight (MW) fit yielded 52,417 Da, compared to the calculated mass of 50,771 Da, for an $MW_{obs}/MW_{calc}$ ratio of 1.03, consistent with a 1:1 heterodimer.

$k_{cat}$ (Table 2). Because the $K_M$ is very similar to that of the unbound UCH37, we considered the possibility that the residual activity results from the presence of some free UCH37 that dissociates from NFRKB under the assay conditions. (In this model, the dissociated UCH37 might be completely unbound, or it may remain bound to regions of NFRKB that do not block substrate binding.) This interpretation was confirmed by active-site titration with ubiquitin aldehyde, which showed that only a minor fraction of UCH37 was reactive (data not shown). Therefore, we conclude that the UCH37-NFRKB complexes are essentially inactive and that the observed residual activity primarily reflects unbound enzyme. Nearly identical observations were found for the NFRKB$^{1–117}$ construct that lacks the C-terminal helix, indicating that, although this interaction likely reinforces inhibition in vivo, its loss does not substantially alter the extent of dissociation under the biochemical assay conditions. Mutation of four of the F100 loop residues ($^{97}$NFRF$^{100}$ to GSGS) resulted in kinetic parameters that are very similar to those of unbound UCH37, likely because this construct is completely released from inhibitory interactions with the UCH domain under the 10-nM assay conditions.

## DISCUSSION

UCH37 is a subunit of the functionally dissimilar proteasome and INO80 complexes. Remarkably, the subunits that recruit UCH37 to these two complexes have opposite effects on UCH37, activating in the case of RPN13/proteasome and inhibiting in the case of NFRKB/INO80. The structural and biochemical findings reported here demonstrate that, in both cases, UCH37 is recruited by binding of its C-terminal domain, especially α10, and that the interactions are highly similar over the first five helices of RPN13$^{CTD}$ and NFRKB$^{NTD}$. Despite this shared binding mechanism with the UCH37$^{CTD}$, RPN13$^{CTD}$ and NFRKB$^{NTD}$ make additional, distinct contacts to the UCH37$^{UCH}$ domain to elicit opposite regulatory effects. RPN13$^{CTD}$ disrupts the inhibitory dimeric structure of UCH37, although this mechanism is unlikely to apply at the concentrations present in vivo, whereas the physiologically relevant contribution of RPN13$^{CTD}$ to UCH37 activation is through stabilization of the substrate-binding conformation. In contrast, NFRKB$^{NTD}$ uses the F100 loop to directly block the ubiquitin L8-binding pocket on UCH37 and stabilizes UCH37 α9 and α10 in positions that further block ubiquitin binding. Moreover, the clasp-like C-terminal helix of NFRKB$^{NTD}$ reinforces the inhibitory binding of the F100 loop and induces a distorted, inactive conformation at the UCH37 active site.

Although our data explain why small ubiquitin adducts such as ubiquitin-AMC are cleaved efficiently by the RPN13 complex, they also raise important mechanistic questions concerning biological function. The role of UCH37 in the proteasome has been debated. One proposal is that UCH37 performs an editing function by removing distal ubiquitin moieties from polyubiquitylated substrates so that inadequately ubiquitylated proteins are released from the proteasome and spared from degradation (Lam et al., 1997). Another proposal is that UCH37

**Table 2. Kinetic Properties of UCH37-Containing Complexes**

| Complexes | $K_M$ (μM) | $k_{cat}$ ($s^{-1}$) | $k_{cat}/K_M$ ($s^{-1}\mu M^{-1}$) |
|---|---|---|---|
| $UCH37^{UCH(1–228)}$ | 23.4 ± 5.2 | 4.6 ± 0.7 | 0.19 ± 0.05 |
| UCH37 | 20.8 ± 4.4 | 3.9 ± 0.5 | 0.19 ± 0.05 |
| UCH37(M269E, N291D) | ND | ND | 0.21 ± 0.01 |
| UCH37/$RPN13^{285–407}$ | 3.1 ± 0.7 | 5.0 ± 0.3 | 1.6 ± 0.4 |
| UCH37(isoform2)/$RPN13^{285–407}$ | 3.3 ± 0.7 | 4.7 ± 0.3 | 1.4 ± 0.3 |
| UCH37(M148A,F149A)/$RPN13^{285–407}$ | 21.7 ± 4.7 | 4.7 ± 0.6 | 0.22 ± 0.05 |
| UCH37/RPN13(Q337A, Q338A)$^{285–407}$ | 7.9 ± 1.2 | 4.7 ± 0.3 | 0.6 ± 0.1 |
| UCH37/$NFRKB^{1–156}$ | 15.4 ± 2.3 | 0.10 ± 0.01 | 0.006 ± 0.001 |
| UCH37/$NFRKB^{39–156}$ | 26.5 ± 4.8 | 0.25 ± 0.03 | 0.009 ± 0.002 |
| UCH37/$NFRKB^{1–156}$ ($^{97}$GSGS$^{100}$) | 20.3 ± 4.8 | 5.94 ± 0.71 | 0.29 ± 0.08 |
| UCH37/$NFRKB^{1–117}$ | 29.2 ± 6.0 | 0.15 ± 0.02 | 0.005 ± 0.001 |

Assays were performed with ubiquitin-AMC. Data are reported as best-fit values with SEs from nonlinear regression fit. All UCH37 constructs used for kinetic analysis refer to human isoform 1 unless otherwise noted. ND, not determined.

deubiquitylates proteasome subunits that can undergo regulatory ubiquitylation (Jacobson et al., 2014). Yet another proposal is that UCH37 might disassemble and, hence, release unanchored polyubiquitin chains that bind avidly to proteasome-associated ubiquitin receptors and thereby block substrate access (Zhang et al., 2011). All of these proposed functions involve the removal of adducts that are at least as large as ubiquitin. Notably, however, the ~20-Å diameter of a maximally open ASCL is insufficient to allow the passage of ubiquitin, which explains the biochemical findings that the $RPN13^{CTD}$ complex fails to efficiently hydrolyze isopeptide bonds in polyubiquitin (Yao et al., 2006). Indeed, we find that diubiquitin processing by UCH37-$RPN13^{CTD}$ is even slower than by UCH37 alone (data not shown), presumably because the open ASCL conformation stabilized by RPN13 impedes access of the large folded substrate, whereas in the absence of RPN13, the ASCL is more mobile and able to flex away from the active site. Our structural data are, therefore, incongruent with leading models of function.

There are several potential explanations for the apparent discrepancy between the structure and proposed substrates: UCH37 may have evolved to act slowly upon its physiological substrates, for example, so that editing is not so efficient that legitimate substrates escape degradation (Lam et al., 1997) or that regulatory ubiquitylation of proteasome subunits is not reversed before a response can be registered. Another possibility is that authentic UCH37 substrates may, in fact, be small ubiquitin adducts, although the identity of those species is not apparent. A third possibility is that the physiologically active conformation might only form upon making additional contacts in the proteasome or activated INO80 complex, although the use of conserved residues at the RPN13 interface indicates that the contacts seen in the crystal structure are physiologically relevant. Indeed, the high degree of conservation seen for residues of the ASCL that remain unstructured in the RPN13-ubiquitin ternary complex suggests that they may play a direct role in recognizing specific substrates, which may be sufficiently flexible to loop through the ASCL while retaining any folded domains on the same side of the ASCL as the bound ubiquitin.

UCH37 is a subunit of metazoan INO80, where it is inactive, presumably because it is bound with NFRKB in the conformation seen in the crystal structure with the ubiquitin-binding site blocked and the active site distorted. The plasticity of UCH domains and the need for ubiquitin-induced conformational changes has been established (Das et al., 2006; Johnston et al., 1997, 1999), but to our knowledge this is the only reported interaction with a specific binding partner that stabilizes an inactive UCH conformation. Incubation of INO80 with isolated RPN13 or the proteasome 19S regulatory particle devoid of UCH37, which presumably displays RPN13 with available UCH37-binding sites, activates INO80-associated UCH37 (Yao et al., 2008). This effect does not cause displacement of UCH37 from INO80 and is lost upon removal of RPN13/proteasome. An attractive scenario is that RPN13 displaces the inhibitory interactions of NFRKB that we see in the crystal structure, whereas additional contacts between UCH37 and NFRKB and/or other INO80 components tether the activated UCH37.

Our observations are consistent with the findings that RPN13 competes with $NFRKB^{1–101}$ for binding to UCH37 (Yao et al., 2008) and that NFRKB residues 1–101 activate UCH37 but that the longer full-length and 1–465 constructs inhibit UCH37 (Yao et al., 2008), as do the 39–156 and 1–117 constructs used in this study. Presumably, binding of $NFRKB^{1–101}$ was activating because it disrupted the UCH37 dimer that is inhibitory in the biochemical assays reported (Yao et al., 2008), but the inhibitory F100 loop is unable to form a stable interaction with the UCH domain when it is unmoored from helix α5 by truncation at residue 101.

Our findings have general relevance for the regulation of the nearly 100 deubiquitylases that are estimated to be encoded by the human genome (Nijman et al., 2005). In particular, UCH37 is most closely related to BAP1, which shares 42% sequence identity over the $UCH37^{UCH}$ domain. The BAP1 UCH domain is followed by a C-terminal extension that is much longer than the $UCH37^{CTD}$ but shares with it a stretch of 68 residues, termed the "ULD" (UCH37-like domain; 34% sequence identity) (Misaghi et al., 2009), that extends over UCH37 residues P246–E313 on helices α9, α10, and α11. Like UCH37, BAP1 associates with a partner protein, ASXL1, which activates BAP1 and is required for the BAP1-mediated deubiquitylation of histone H2A in nucleosomes (Scheuermann et al., 2010). Notably, an informatics study (Sanchez-Pulido et al., 2012) proposed that the UCH37 and BAP1 ULDs interact with the DEUBAD (deubiquitylase adaptor) domains of RPN13 and NFRKB and of ASXL1, respectively. These DEUBAD sequences cover essentially the entire $RPN13^{CTD}$ and $NFRKB^{NTD}$ structures of our UCH37 complexes, which strongly implies that the corresponding DEUBAD residues of ASXL1 will bind BAP1 in the same manner as the first five helices of $RPN13^{CTD}$ and $NFRKB^{NTD}$. The UCH37 and BAP1 ASCL residues do not share obvious sequence similarity, although like UCH37, the ASCL residues are remarkably conserved between BAP1 homologs, including multiple residues that are flexible and lack electron density in all of the UCH37

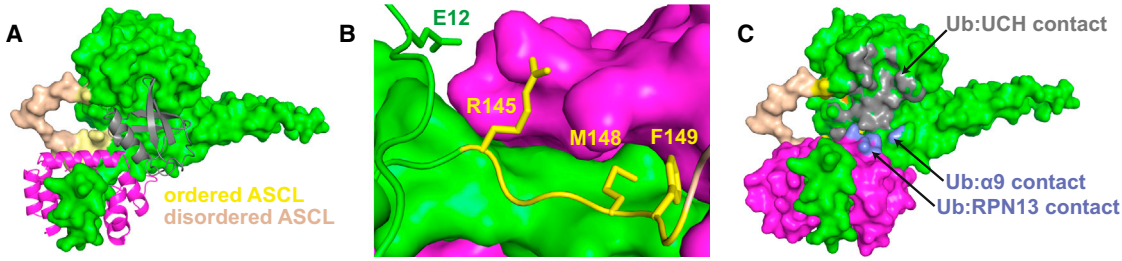


**Figure 4. Activation of UCH37 by RPN13**

(A) Structure of the UCH37-RPN13-ubiquitin complex.

(B) RPN13 contacts with ASCL residues.

(C) Ubiquitin contact surfaces. Similar orientation to (A).

structures. This suggests that these residues play functionally important roles that have yet to be defined but may include binding of specific substrates or regions of partner proteins within their respective UCH37 and BAP1 complexes.

The structural and biochemical insights from this work provide a foundation for future studies to understand the complicated biology of the essential UCH37 enzyme. These include the design of experiments to (1) delineate the distinct physiological roles of UCH37 in the proteasome and in INO80; (2) determine the authentic, physiologically relevant substrates in each context; and (3) determine the mechanistic basis for dynamic regulation of UCH37 in INO80, where association with RPN13 or proteasome can stimulate activity. A genome-wide RNAi screen identified NFRKB and other INO80 subunits among the top hits required for the maintenance of human embryonic stem cell identity (Chia et al., 2010). It will be of great interest to determine whether UCH37 also functions in this context and whether this is the cause of the early embryonic lethality of *Uch37* null mice (Al-Shami et al., 2010). A recent report (Nishi et al., 2014) that UCH37 and NFRKB are relevant for DNA double-strand break repair by homologous recombination adds further interest to the question of physiological substrate(s) and mechanism of activation. It will also be important to determine the basis for binding and recruitment of UCH37 to a third distinct complex centered on SMAD7 (Wicks et al., 2006) and further delineate how distinct binding partners impart tight regulation and unique substrate specificity to the same catalytic subunit.

## EXPERIMENTAL PROCEDURES

### Protein Expression Constructs

Details of expression plasmids are given in Table S1. Human *UCH37* (isoform 1) and murine *Uch37* (isoform 2) cDNAs were inserted into pET151 vectors (Invitrogen) from pET41a-hUch37 and cDNA (ATCC:MGC-6295), respectively. $UCH37^{DM}$, UCH37(M148A/F149A), and RPN13(Q337A/Q338A) were engineered by QuickChange mutagenesis. $UCH37^{UCH(1–228)}$ was engineered by insertion of a stop codon into the hUCH37 (isoform 1) construct. $RPN13^{285–407}$ was amplified from *RPN13* cDNA (isoform 1) and inserted into pDEST15. Because $RPN13^{285–407}$ contains only a single tyrosine, the phenylalanine residue in the GSFT sequence that remains following tobacco etch virus (TEV) protease treatment was changed to a tryptophan (renaming the plasmid pDEST15.1) to facilitate quantification. The expression vector for $RPN13^{285–386}$ was engineered by insertion of a stop codon into the $RPN13^{285–407}$ construct. Human UCH37 isoform 2 was engineered by deleting the codon for E246 from human UCH37 isoform 1. Human $NFRKB^{1–156}$, $NFRKB^{39–156}$, and $NFRKB^{1–117}$ were amplified from pcDNA5-Flag-NFRKB (Yao et al., 2008). For expression of UCH37-NFRKB complexes, human *UCH37* and *NFRKB* were inserted into the MCS1 and MCS2 sites of a pETDUET-1 vector (Invitrogen).

### UCH37 and RPN13 Expression and Purification

Purifications were performed at 4°C except where noted. UCH37 and RPN13 constructs were expressed in BL21(DE3) codon+ (RIL) *E. coli* cells (Stratagene) in autoinduction media ZYP-5052 (Studier, 2005) at 37°C to an optical density 600 ($OD_{600}$) of ~1.0 and then transferred to 19°C for 20 hr. Cultures were harvested by centrifugation and stored at −80°C, with cultures destined for preparation of RPN13-UCH37 complexes mixed 1:1 (volume) prior to harvesting. Pellets were resuspended in lysis buffer (20 mM Tris-HCl [pH 7.5], 300 mM NaCl, and 10 mM imidazole) supplemented with 0.5% Triton X-100 and protease inhibitors (leupeptin, pepstatin, aprotinin, PMSF) (Sigma) and sonicated. Lysate was clarified by centrifugation.

UCH37-RPN13 complexes were purified in five chromatographic steps. (1) Clarified lysate was incubated with Ni-NTA resin (QIAGEN) for 1 hr, washed with 20 column volumes (CV) of lysis buffer, and eluted with 5 CV Ni lysis buffer plus 240 mM imidazole, 1 mM DTT, and 1 mM EDTA. (2) Eluate was incubated with glutathione sepharose resin (GE Healthcare) for 1 hr, washed with 10 CV of GS-BIND buffer (20 mM Tris-HCl [pH 7.4], 50 mM NaCl, 1 mM DTT, and 1 mM EDTA), incubated with TEV protease (0.005 mg/ml), and eluted with GS-BIND buffer. (3) Eluate was loaded on a HiTrap Q HP column (GE Healthcare), washed with 10 CV of QA buffer (20 mM Tris-HCl [pH 7.5], 10 mM imidazole), and eluted with a gradient of 0–400 mM NaCl over 20 CV. (4) Eluate was incubated with Ni-NTA resin pre-equilibrated in QA buffer. (5) The flowthrough was concentrated and run on a Superdex 200 (GE Healthcare) gel filtration column in 20 mM HEPES [pH 7.2], 100 mM NaCl, 1 mM TCEP, and 1 mM EDTA.

Minor modifications were used for the purification of isolated UCH37 and RPN13. For isolated UCH37, step 1 included 40 mM imidazole in the wash buffer, and step 2 was substituted with incubation of the Ni-NTA eluate with TEV protease followed by overnight dialysis in GS Bind Buffer. For isolated RPN13, steps 1 and 4 were omitted.

Human ubiquitin was expressed and purified as described elsewhere (Pickart and Raasi, 2005).

### NFRKB Expression and Purification

The UCH37-NFRKB complexes were expressed in BL21(DE3) codon+ (RIL) *E. coli* cells (Stratagene) in LB media. Cells were grown at 37°C to an $OD_{600}$ of 0.6–0.8 and induced with 0.5 mM IPTG for either 3 hr at 37°C or 20 hr at 19°C. Cultures were harvested by centrifugation and stored at −80°C. Pellets were resuspended in lysis buffer (2× PBS, 10 mM imidazole, and 10 mM β-mercaptoethanol [BME]) supplemented with protease inhibitors (leupeptin, pepstatin, aprotinin, PMSF) (Sigma) and treated with 100 μg/ml lysozyme for 30 min prior to sonication. Lysate was clarified by centrifugation.

UCH37-NFRKB complexes were purified in four chromatographic steps. (1) Clarified lysate was incubated with Ni-NTA resin (QIAGEN) for 1 hr, washed with 10 CV of lysis buffer, washed with 10 CV of lysis buffer plus 10 mM imidazole, and eluted with 7 CV of lysis buffer plus 240 mM imidazole. (2) Eluate

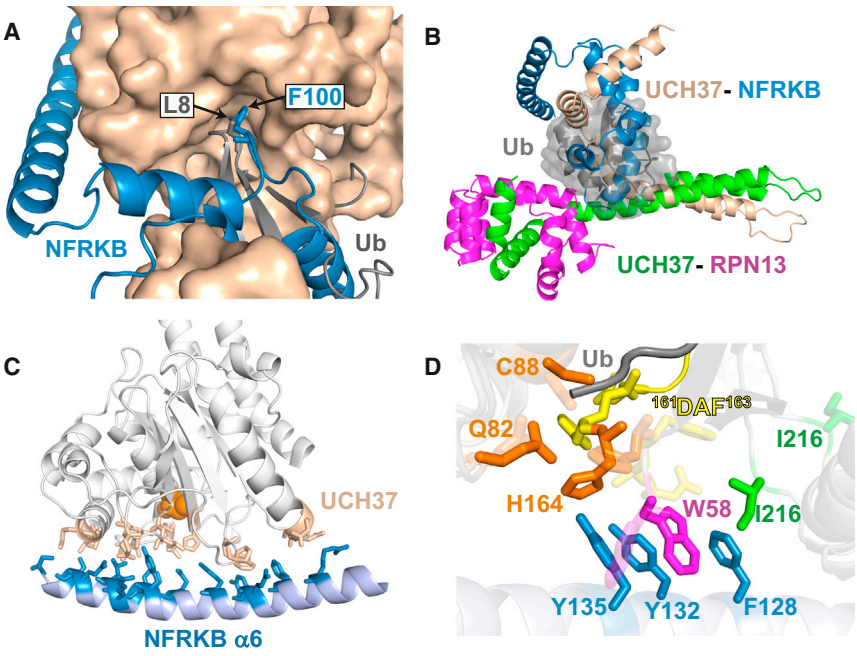


**Figure 5. Inhibition of UCH37 by NFRKB**

(A) The L8 loop of ubiquitin and the F100 loop of NFRKB bind to the same pocket on UCH37.

(B) Ribbon diagram, same as in Figure 3B but including RPN13, NFRKB, and ubiquitin.

(C) Contacts of the NFRKB C-terminal helix with the $UCH37^{UCH}$ domain.

(D) Superposition of the UCH37 active sites for the NFRKB-bound inactive conformation (solid) and the RPN13-bound active conformation (semitransparent) following overlap on the UCH domains. Residues on the NFRKB C-terminal helix are colored blue.

was incubated overnight at 4°C with PreScission protease (0.005 mg/ml) in the presence of 1 mM DTT, dialyzed into lysis buffer, and incubated with Ni-NTA resin equilibrated with lysis buffer. (3) Flowthrough was dialyzed into QA buffer (20 mM Tris-HCl [pH 7.5], 50 mM NaCl) and loaded on a HiTrap Q HP column, washed with 10 CV of QA buffer, and eluted with a gradient of 50–400 mM NaCl over 30 CV. (4) Eluted protein fractions were concentrated (3K MWCO Vivaspin Centrifugal Concentrator) and run on a Superdex 200 gel filtration column in 20 mM HEPES [pH 7.2], 100 mM NaCl, 1 mM TCEP, and 1 mM EDTA.

### Crystallization and Structure Determination

Gel filtration fractions were concentrated for crystallization. All UCH37-RPN13 crystals were grown in sitting drops of 2:1 protein:reservoir at 4°C. UCH37-$RPN13^{285–386}$ (12 mg/ml) was crystallized against a reservoir of 20% polyethylene glycol (PEG) 3350, 0.2 M $Mg(OAc)_2$, and 0.1 HEPES (pH 7.3). The ternary complex was prepared by mixing purified UCH37-$RPN13^{285–386}$ and ubiquitin 1:1.2 to a final concentration of 12 mg/ml and crystallized against a reservoir solution of 25% PEG 3350, 0.2 M $MgCl_2$, and 0.1 M Bis-Tris (pH 6.6). UCH37-$NFRKB^{39–156}$ crystals were grown in hanging drops of 2:1 or 2:2 protein:reservoir at 20°C against a reservoir of 16%–18% PEG 3350 and 100–300 mM ammonium citrate (pH 7.0), using 10–12 mg/ml protein complex.

Crystals were immersed briefly in reservoir solution made up with 20% glycerol and cryocooled for data collection by plunging into liquid nitrogen. Diffraction data were collected on a Rigaku R-AXIS IV at 1.54 Å wavelength (UCH37-$RPN13^{285–386}$), on NSLS beamline X-29 (UCH37-$RPN13^{285–386}$-ubiquitin) at a 1.075-Å wavelength with a Q315 detector or on SSRL beamline 11-1 (UCH37-$NFRKB^{39–156}$) at a 0.97945-Å wavelength with a Pilatus 6M detector. Data were processed using XDS (Kabsch, 2010). Phases were determined by molecular replacement with Phaser-MR (McCoy et al., 2007) using the UCH domain of UCH37 as a search model. Models were built with COOT (Emsley et al., 2010) and refined with PHENIX (Adams et al., 2010). PyMOL (The PyMOL Molecular Graphics System, Version 1.5.0.4, Schrödinger, LLC) was used to make molecular structure figures and to define contact surfaces.

Model geometries were analyzed by MolProbity (Chen et al., 2010a) within PHENIX. For the UCH37-$RPN13^{285–386}$ model, 96.1% of residues have favorable backbone dihedrals, 3.6% fall into allowed regions, and 0.3% are outliers. Residues 1–5, 151–161, and 248–253 of UCH37 and residues 285, 385, and 386 of RPN13 are not visible in the electron density. For the ternary UCH37-$RPN13^{285–386}$-ubiquitin model, 98.5% of residues have favored backbone dihedrals, whereas 1.5% fall into the allowed regions. Residues 1–5, 151–160, and 247–253 of UCH37 and residues 285, 385, and 386 of RPN13 are not visible in the electron density. For the UCH37-$NFRKB^{39–156}$ model, 96.8% of backbone dihedrals fall within the favored region, 2.5% fall into allowed regions, and 0.7% are outliers. Residues 1–4, 149–157, and 242–253 of UCH37 and residues 39 and 154–156 of NFRKB are not visible in the electron density.

### Equilibrium AUC

AUC data were collected at 4°C using an Optima XL-A centrifuge and An-60 Ti rotor (Beckman Coulter). Samples in 20 mM HEPES (pH 7.5), 0.5 mM EDTA, and 1 mM TCEP were centrifuged at either 7,000, 9,000, and 13,000 rpm (hUCH37 isoform 1 and $UCH37^{DM}$) or 9,000, 11,000, and 13,000 rpm ($UCH37^{UCH(1–228)}$ and UCH37-$RPN13^{CTD}$), with initial protein concentrations of 8, 4, and 2 μM for full-length UCH37 constructs and 20, 10, and 5 μM for $UCH37^{UCH(1–228)}$. Data were globally fit to ideal single-species models with floating molecular masses ($UCH37^{UCH(1–228)}$ and UCH37-$RPN13^{285–407}$) or to monomer-dimer equilibrium models (hUCH37 and $UCH37^{DM}$) using HETEROANALYSIS (Cole, 2004). Protein partial specific volumes and solvent densities were calculated with the program SEDNTERP 1.09 (Laue et al., 1992). Data for isoforms 1 and 2 of UCH37 were indistinguishable under these conditions. Equivalent experiments were performed in the presence of 150 mM NaCl and, in all cases, gave protein association constants that were the same within experimental error. Some aggregation of hUCH37 isoform 1, hUCH37 isoform 2, and $UCH37^{DM}$ was apparent in the presence of 150 mM NaCl, at the concentrations described earlier, although $UCH37^{UCH(1–228)}$, UCH37 isoform 1-$RPN13^{CTD}$, and UCH37 isoform 2-$RPN13^{CTD}$ did not aggregate and fit well to ideal single species at the expected molecular weights. Additional experiments at lower protein concentrations (2.5 μM, 1.25 μM, 600 nM) used absorbance at 230 nm and a buffer that minimized background absorption (20 mM sodium phosphate [pH 7.5], 150 mM NaCl, 0.05 mM EDTA, 0.1 mM TCEP). Aggregation was still observed for hUCH37 isoform 1, hUCH37 isoform 2, and $UCH37^{DM}$ in the 2.5-μM sample, although data from the 1.25 μM and 600 nM samples collected at four speeds (7,000, 9,000, 13,000, and 16,000 rpm) fit well to a monomer-dimer equilibrium, with $K_D$ values in close agreement with our other analyses.

### Ubiquitin-AMC Assays

Enzyme concentrations were determined by densitometry measurements from Coomassie-stained gels using UCH37 as a standard. Concentrations of $UCH37^{UCH(1–228)}$ were estimated by absorbance at 280 nm and confirmed by active-site titration experiments with ubiquitin-aldehyde. Ubiquitin-AMC (BostonBiochem or UbiQ) hydrolysis was monitored continuously for 1 hr at 30°C on a fluorescence plate reader (BioTek Synergy 4, $\lambda_{excitation}$ = 340 nm and $\lambda_{emission}$ = 440 nm); initial velocities of fluorescence increases were converted to concentration of AMC released per second by reference to an AMC standard. Reactions were performed in assay buffer (50 mM HEPES [pH 7.5], 150 mM NaCl, 0.5 mM EDTA, 5 mM DTT, and 1 mg/ml ovalbumin) and typically contained 1 nM enzyme for the active complexes or 10 nM for the NFRKB-containing complexes. Data were fit with the Michaelis-Menten

equation using PRISM (GraphPad Software). At a minimum, duplicated reactions were performed for each experiment. Best-fit values and SEs from the fitting are reported. UCH37 isoform 1 gave good data under all conditions reported. Unbound isoform 2 appeared to suffer from aggregation, although kinetic parameters of the UCH37 isoform 2-RPN13 complex were indistinguishable from the isoform 1 complex.

## ACCESSION NUMBERS

Coordinates and structure factor amplitudes have been deposited at the PDB under the accession ID codes 4WLP (UCH37-NFRKB), 4WLQ (UCH37-RPN13), and 4WLR (UCH37-RPN13-ubiquitin).

## SUPPLEMENTAL INFORMATION

Supplemental Information includes one table and can be found with this article online at http://dx.doi.org/10.1016/j.molcel.2015.01.016.

## AUTHOR CONTRIBUTIONS

R.E.C., T.Y., and C.P.H. designed the experiments. R.T.V., C.W.H., B.S., and A.N. conducted the experiments. F.G.W. and H.R. made important contributions to the X-ray crystallography experiments. R.T.V., C.W.H., R.E.C., T.Y., and C.P.H. wrote the paper.

## ACKNOWLEDGMENTS

We thank Heidi L. Schubert and Debra M. Eckert for expert technical advice and helpful comments on the manuscript and Katherine Ferrell and Binita Shakya for technical assistance. Portions of this research were performed at the National Synchrotron Light Source (NSLS) and the Stanford Synchrotron Radiation Lightsource (SSRL). The NSLS is funded by the National Center for Research Resources (NCRR) (P41RR012408). The SSRL Structural Molecular Biology Program is supported by the Department of Energy (DOE) Office of Biological and Environmental Research and by the NIH, National Institute of General Medical Sciences (NIGMS) (including P41GM103393), and the NCRR (P41RR001209). Use of the NSLS and SSRL is supported by the DOE Office of Basic Energy Sciences (SSRL Contract No. DE-AC02-76SF00515). NSLS operations are also supported by the NIH. The contents of this publication are solely the responsibility of the authors and do not necessarily represent the official views of NIGMS, NCRR, or NIH. This work was supported by NIH grants R01 GM059135 and P50 GM082545 to C.P.H., R01 GM098401 to T.Y., and R01 GM097452 to R.E.C. Mass spectrometry validation of purified proteins was performed by the University of Utah Mass Spectrometry and Proteomics Core Facility, which is supported by P30CA042014 from the National Cancer Institute.

Received: October 9, 2014
Revised: December 15, 2014
Accepted: January 6, 2015
Published: February 19, 2015

## REFERENCES

Adams, P.D., Afonine, P.V., Bunkóczi, G., Chen, V.B., Davis, I.W., Echols, N., Headd, J.J., Hung, L.W., Kapral, G.J., Grosse-Kunstleve, R.W., et al. (2010). PHENIX: a comprehensive Python-based system for macromolecular structure solution. Acta Crystallogr. D Biol. Crystallogr. *66*, 213–221.

Al-Shami, A., Jhaver, K.G., Vogel, P., Wilkins, C., Humphries, J., Davis, J.J., Xu, N., Potter, D.G., Gerhardt, B., Mullinax, R., et al. (2010). Regulators of the proteasome pathway, Uch37 and Rpn13, play distinct roles in mouse development. PLoS ONE *5*, e13654.

Artavanis-Tsakonas, K., Weihofen, W.A., Antos, J.M., Coleman, B.I., Comeaux, C.A., Duraisingh, M.T., Gaudet, R., and Ploegh, H.L. (2010). Characterization and structural studies of the Plasmodium falciparum ubiquitin and Nedd8 hydrolase UCHL3. J. Biol. Chem. *285*, 6857–6866.

Boudreaux, D.A., Maiti, T.K., Davies, C.W., and Das, C. (2010). Ubiquitin vinyl methyl ester binding orients the misaligned active site of the ubiquitin hydrolase UCHL1 into productive conformation. Proc. Natl. Acad. Sci. USA *107*, 9117–9122.

Burgie, S.E., Bingman, C.A., Soni, A.B., and Phillips, G.N., Jr. (2012). Structural characterization of human Uch37. Proteins *80*, 649–654.

Cai, Y., Jin, J., Yao, T., Gottschalk, A.J., Swanson, S.K., Wu, S., Shi, Y., Washburn, M.P., Florens, L., Conaway, R.C., and Conaway, J.W. (2007). YY1 functions with INO80 to activate transcription. Nat. Struct. Mol. Biol. *14*, 872–874.

Chen, V.B., Arendall, W.B., 3rd, Headd, J.J., Keedy, D.A., Immormino, R.M., Kapral, G.J., Murray, L.W., Richardson, J.S., and Richardson, D.C. (2010a). MolProbity: all-atom structure validation for macromolecular crystallography. Acta Crystallogr. D Biol. Crystallogr. *66*, 12–21.

Chen, X., Lee, B.H., Finley, D., and Walters, K.J. (2010b). Structure of proteasome ubiquitin receptor hRpn13 and its activation by the scaffolding protein hRpn2. Mol. Cell *38*, 404–415.

Chen, Y., Fu, D., Xi, J., Ji, Z., Liu, T., Ma, Y., Zhao, Y., Dong, L., Wang, Q., and Shen, X. (2012). Expression and clinical significance of UCH37 in human esophageal squamous cell carcinoma. Dig. Dis. Sci. *57*, 2310–2317.

Chen, Y.J., Ma, Y.S., Fang, Y., Wang, Y., Fu, D., and Shen, X.Z. (2013). Power and promise of ubiquitin carboxyl-terminal hydrolase 37 as a target of cancer therapy. Asian Pac. J. Cancer Prev. *14*, 2173–2179.

Chia, N.Y., Chan, Y.S., Feng, B., Lu, X., Orlov, Y.L., Moreau, D., Kumar, P., Yang, L., Jiang, J., Lau, M.S., et al. (2010). A genome-wide RNAi screen reveals determinants of human embryonic stem cell identity. Nature *468*, 316–320.

Clague, M.J., Coulson, J.M., and Urbé, S. (2012). Cellular functions of the DUBs. J. Cell Sci. *125*, 277–286.

Cole, J.L. (2004). Analysis of heterogeneous interactions. Methods Enzymol. *384*, 212–232.

Cutts, A.J., Soond, S.M., Powell, S., and Chantry, A. (2011). Early phase TGFβ receptor signalling dynamics stabilised by the deubiquitinase UCH37 promotes cell migratory responses. Int. J. Biochem. Cell Biol. *43*, 604–612.

D'Arcy, P., Brnjic, S., Olofsson, M.H., Fryknäs, M., Lindsten, K., De Cesare, M., Perego, P., Sadeghi, B., Hassan, M., Larsson, R., and Linder, S. (2011). Inhibition of proteasome deubiquitinating activity as a new cancer therapy. Nat. Med. *17*, 1636–1640.

Das, C., Hoang, Q.Q., Kreinbring, C.A., Luchansky, S.J., Meray, R.K., Ray, S.S., Lansbury, P.T., Ringe, D., and Petsko, G.A. (2006). Structural basis for conformational plasticity of the Parkinson's disease-associated ubiquitin hydrolase UCH-L1. Proc. Natl. Acad. Sci. USA *103*, 4675–4680.

Emsley, P., Lohkamp, B., Scott, W.G., and Cowtan, K. (2010). Features and development of Coot. Acta Crystallogr. D Biol. Crystallogr. *66*, 486–501.

Fabrini, R., De Luca, A., Stella, L., Mei, G., Orioni, B., Ciccone, S., Federici, G., Lo Bello, M., and Ricci, G. (2009). Monomer-dimer equilibrium in glutathione transferases: a critical re-examination. Biochemistry *48*, 10473–10482.

Fang, Y., Mu, J., Ma, Y., Ma, D., Fu, D., and Shen, X. (2012). The interaction between ubiquitin C-terminal hydrolase 37 and glucose-regulated protein 78 in hepatocellular carcinoma. Mol. Cell. Biochem. *359*, 59–66.

Hamazaki, J., Iemura, S., Natsume, T., Yashiroda, H., Tanaka, K., and Murata, S. (2006). A novel proteasome interacting protein recruits the deubiquitinating enzyme UCH37 to 26S proteasomes. EMBO J. *25*, 4524–4536.

Holm, L., and Rosenström, P. (2010). Dali server: conservation mapping in 3D. Nucleic Acids Res. *38*, W545–W549.

Hölzl, H., Kapelari, B., Kellermann, J., Seemüller, E., Sümegi, M., Udvardy, A., Medalia, O., Sperling, J., Müller, S.A., Engel, A., and Baumeister, W. (2000). The regulatory complex of Drosophila melanogaster 26S proteasomes. Subunit composition and localization of a deubiquitylating enzyme. J. Cell Biol. *150*, 119–130.

Jacobson, A.D., MacFadden, A., Wu, Z., Peng, J., and Liu, C.W. (2014). Autoregulation of the 26S proteasome by in situ ubiquitination. Mol. Biol. Cell *25*, 1824–1835.

Jiao, L., Ouyang, S., Shaw, N., Song, G., Feng, Y., Niu, F., Qiu, W., Zhu, H., Hung, L.W., Zuo, X., et al. (2014). Mechanism of the Rpn13-induced activation of Uch37. Protein Cell *5*, 616–630.

Johnston, S.C., Larsen, C.N., Cook, W.J., Wilkinson, K.D., and Hill, C.P. (1997). Crystal structure of a deubiquitinating enzyme (human UCH-L3) at 1.8 A resolution. EMBO J. *16*, 3787–3796.

Johnston, S.C., Riddle, S.M., Cohen, R.E., and Hill, C.P. (1999). Structural basis for the specificity of ubiquitin C-terminal hydrolases. EMBO J. *18*, 3877–3887.

Kabsch, W. (2010). XDS. Acta Crystallogr. D Biol. Crystallogr. *66*, 125–132.

Lam, Y.A., Xu, W., DeMartino, G.N., and Cohen, R.E. (1997). Editing of ubiquitin conjugates by an isopeptidase in the 26S proteasome. Nature *385*, 737–740.

Laue, T.M., Shah, B.D., Ridgeway, T.M., and Pelletier, S.L., eds. (1992). Analytical ultracentrifugation in biochemistry and polymer science (Royal Society of Chemistry).

Li, T., Naqvi, N.I., Yang, H., and Teo, T.S. (2000). Identification of a 26S proteasome-associated UCH in fission yeast. Biochem. Biophys. Res. Commun. *272*, 270–275.

Maiti, T.K., Permaul, M., Boudreaux, D.A., Mahanic, C., Mauney, S., and Das, C. (2011). Crystal structure of the catalytic domain of UCHL5, a proteasome-associated human deubiquitinating enzyme, reveals an unproductive form of the enzyme. FEBS J. *278*, 4917–4926.

McCoy, A.J., Grosse-Kunstleve, R.W., Adams, P.D., Winn, M.D., Storoni, L.C., and Read, R.J. (2007). Phaser crystallographic software. J. Appl. Crystallogr. *40*, 658–674.

Misaghi, S., Galardy, P.J., Meester, W.J., Ovaa, H., Ploegh, H.L., and Gaudet, R. (2005). Structure of the ubiquitin hydrolase UCH-L3 complexed with a suicide substrate. J. Biol. Chem. *280*, 1512–1520.

Misaghi, S., Ottosen, S., Izrael-Tomasevic, A., Arnott, D., Lamkanfi, M., Lee, J., Liu, J., O'Rourke, K., Dixit, V.M., and Wilson, A.C. (2009). Association of C-terminal ubiquitin hydrolase BRCA1-associated protein 1 with cell cycle regulator host cell factor 1. Mol. Cell. Biol. *29*, 2181–2192.

Morrow, M.E., Kim, M.I., Ronau, J.A., Sheedlo, M.J., White, R.R., Chaney, J., Paul, L.N., Lill, M.A., Artavanis-Tsakonas, K., and Das, C. (2013). Stabilization of an unusual salt bridge in ubiquitin by the extra C-terminal domain of the proteasome-associated deubiquitinase UCH37 as a mechanism of its exo specificity. Biochemistry *52*, 3564–3578.

Nijman, S.M., Luna-Vargas, M.P., Velds, A., Brummelkamp, T.R., Dirac, A.M., Sixma, T.K., and Bernards, R. (2005). A genomic and functional inventory of deubiquitinating enzymes. Cell *123*, 773–786.

Nishi, R., Wijnhoven, P., le Sage, C., Tjeertes, J., Galanty, Y., Forment, J.V., Clague, M.J., Urbé, S., and Jackson, S.P. (2014). Systematic characterization of deubiquitylating enzymes for roles in maintaining genome integrity. Nat. Cell Biol. *16*, 1016–1026, 1–8.

Nishio, K., Kim, S.W., Kawai, K., Mizushima, T., Yamane, T., Hamazaki, J., Murata, S., Tanaka, K., and Morimoto, Y. (2009). Crystal structure of the de-ubiquitinating enzyme UCH37 (human UCH-L5) catalytic domain. Biochem. Biophys. Res. Commun. *390*, 855–860.

Pickart, C.M. (2001). Ubiquitin enters the new millennium. Mol. Cell *8*, 499–504.

Pickart, C.M., and Raasi, S. (2005). Controlled synthesis of polyubiquitin chains. Methods Enzymol. *399*, 21–36.

Qiu, X.B., Ouyang, S.Y., Li, C.J., Miao, S., Wang, L., and Goldberg, A.L. (2006). hRpn13/ADRM1/GP110 is a novel proteasome subunit that binds the deubiquitinating enzyme, UCH37. EMBO J. *25*, 5742–5753.

Sanchez-Pulido, L., Kong, L., and Ponting, C.P. (2012). A common ancestry for BAP1 and Uch37 regulators. Bioinformatics *28*, 1953–1956.

Scheuermann, J.C., de Ayala Alonso, A.G., Oktaba, K., Ly-Hartig, N., McGinty, R.K., Fraterman, S., Wilm, M., Muir, T.W., and Müller, J. (2010). Histone H2A deubiquitinase activity of the Polycomb repressive complex PR-DUB. Nature *465*, 243–247.

Studier, F.W. (2005). Protein production by auto-induction in high density shaking cultures. Protein Expr. Purif. *41*, 207–234.

Varshavsky, A. (2005). Regulated protein degradation. Trends Biochem. Sci. *30*, 283–286.

Wang, L., Chen, Y.J., Xu, K., Wang, Y.Y., Shen, X.Z., and Tu, R.Q. (2014). High expression of UCH37 is significantly associated with poor prognosis in human epithelial ovarian cancer. Tumour Biol. *11*, 11427–11433.

Weiss, J.M. (2001). Global indicators of X-ray data quality. Journal of Appl. Crystallogr. *34*, 130–135.

Wicks, S.J., Grocott, T., Haros, K., Maillard, M., ten Dijke, P., and Chantry, A. (2006). Reversible ubiquitination regulates the Smad/TGF-beta signalling pathway. Biochem. Soc. Trans. *34*, 761–763.

Wu, S., Shi, Y., Mulligan, P., Gay, F., Landry, J., Liu, H., Lu, J., Qi, H.H., Wang, W., Nickoloff, J.A., et al. (2007). A YY1-INO80 complex regulates genomic stability through homologous recombination-based repair. Nat. Struct. Mol. Biol. *14*, 1165–1172.

Yao, T., Song, L., Xu, W., DeMartino, G.N., Florens, L., Swanson, S.K., Washburn, M.P., Conaway, R.C., Conaway, J.W., and Cohen, R.E. (2006). Proteasome recruitment and activation of the Uch37 deubiquitinating enzyme by Adrm1. Nat. Cell Biol. *8*, 994–1002.

Yao, T., Song, L., Jin, J., Cai, Y., Takahashi, H., Swanson, S.K., Washburn, M.P., Florens, L., Conaway, R.C., Cohen, R.E., and Conaway, J.W. (2008). Distinct modes of regulation of the Uch37 deubiquitinating enzyme in the proteasome and in the Ino80 chromatin-remodeling complex. Mol. Cell *31*, 909–917.

Zhang, N.Y., Jacobson, A.D., Macfadden, A., and Liu, C.W. (2011). Ubiquitin chain trimming recycles the substrate binding sites of the 26 S proteasome and promotes degradation of lysine 48-linked polyubiquitin conjugates. J. Biol. Chem. *286*, 25540–25546.

**Molecular Cell**

**Supplemental Information**

# Structural Basis for the Activation and Inhibition of the UCH37 Deubiquitylase

**Ryan T. VanderLinden, Casey W. Hemmis, Benjamin Schmitt, Ada Ndoja, Frank G. Whitby, Howard Robinson, Robert E. Cohen, Tingting Yao, and Christopher P. Hill**

## Table S1. Expression plasmids

| Plasmid | Protein(s) | Source | Accession # |
|---|---|---|---|
| pET151-mUCH37 (ISF2) | 6xHIS-TEV-mUCH37 (isoform 2) | M.musculus | NP_001153338 |
| pET151-hUCH37 (ISF1) | 6xHIS-TEV-hUCH37 (isoform 1) | H.sapiens | NP_057068 |
| pET151-hUCH37 (ISF2) | 6xHIS-TEV-hUCH37 (isoform 2) | H.sapiens | NP_001186190 |
| pET151-hUCH37$^{DM}$ | 6xHIS-TEV-hUCH37 (M269E/N291D) (isoform 1) | H.sapiens | NP_057068 |
| pET151-hUCH37$^{UCH(1-228)}$ | 6xHIS-TEV-hUCH37 (1-228) | H.sapiens | NP_057068 |
| pET151-hUCH37(M148A/F149A) | 6xHIS-TEV-hUCH37 (M148A/F149A) (isoform 1) | H.sapiens | NP_057068 |
| pDEST15.1-hRPN13$^{285-407}$ | GST-TEV-GSWT-hRPN13 (285-407) | H.sapiens | NP_008933 |
| pDEST15.1-hRPN13$^{285-407}$ (Q337A/Q338A) | GST-TEV-GSWT-hRPN13 (285-407) (Q337A/Q338A) | H.sapiens | NP_008933 |
| pDEST15.1-hRPN13$^{285-386}$ | GST-TEV-GSWT-hRPN13 (285-386) | H.sapiens | NP_008933 |
| pET3a-hUb | Human ubiquitin | H.sapiens | NP_066289.3 |
| pETDUET1-hUCH37 (ISF1) - NFRKB$^{39-156}$ | 6xHIS -hUCH37 (isoform 1)<br>hNFRKB (39-156) | H.sapiens<br>H.sapiens | NP_057068<br>NP_001137307 |
| pETDUET1-hUCH37 (ISF2) - NFRKB$^{39-156}$ | 7xHIS-PP-hUCH37 (isoform 2)<br>hNFRKB (39-156) | H.sapiens<br>H.sapiens | NP_001186190<br>NP_001137307 |
| pETDUET1-hUCH37-NFRKB$^{1-156}$ | 6xHIS- hUCH37 (isoform 1)<br>hNFRKB (1-156) | H.sapiens<br>H.sapiens | NP_057068<br>NP_001137307 |
| pETDUET1-hUCH37-NFRKB$^{1-156}$(GSGS) | 6xHIS -hUCH37 (isoform 1)<br>hNFRKB (1-156) $^{97}$NFRF$^{100}$/$^{97}$GSGS$^{100}$ | H.sapiens<br>H.sapiens | NP_057068<br>NP_001137307 |
| pETDUET1-hUCH37-NFRKB$^{(1-117)}$ | 6xHIS -hUCH37 (isoform 1)<br>hNFRKB (1-117) | H.sapiens<br>H.sapiens | NP_057068<br>NP_001137307 |

**TEV**-TEV protease recognition sequence, **PP**-PreScission protease recognition sequence
Plasmids have been deposited to the Addgene plasmid repository (www.addgene.org).